

Copyright Protection for 3D Molecular Structures with Watermarking

Runwen Hu¹, Peilin Chen¹, Keyan Ding², and Shiqi Wang^{1,*}

¹Department of Computer Science, City University of Hong Kong, Hong Kong (SAR), China

²ZJU-Hangzhou Global Scientific and Technological Innovation Center, Zhejiang University, Hangzhou, China

*corresponding author: Shiqi Wang

e-mail: runwenhu@cityu.edu.hk; plchen3@cityu.edu.hk; dingkeyan@zju.edu.cn; shiqiwan@cityu.edu.hk

ABSTRACT

Artificial intelligence (AI) revolutionizes molecule generation in bioengineering and biological research, significantly accelerating discovery processes. However, this advancement introduces critical concerns regarding intellectual property protection. To address these challenges, we propose the first robust watermarking method designed for molecules, which utilizes atom-level features to preserve molecular integrity and invariant features to ensure robustness against affine transformations. Comprehensive experiments validate the effectiveness of our method using the datasets QM9 and GEOM-DRUG, and generative models GeoBFN and GeoLDM. We demonstrate the feasibility of embedding watermarks, maintaining basic properties higher than 90.00% while achieving watermark accuracy greater than 95.00%. Furthermore, downstream docking simulations reveal comparable performance between original and watermarked molecules, with binding affinities reaching -6.00 kcal/mol and root mean square deviations below 1.602 Å. These results confirm that our watermarking technique effectively safeguards molecular intellectual property without compromising scientific utility, enabling secure and responsible AI integration in molecular discovery and research applications.

Synthetic molecules are crucial in biological, chemical, and medical research, benefiting scientific discoveries such as protein engineering^{1,2} and drug discovery^{3,4}. The development of artificial intelligence (AI) has significantly facilitated molecule design, establishing a new paradigm for biomedical and biochemical research⁵. Recent progress in AI-based generative models has catalyzed substantial advancements in molecule generation. For example, Gebauer *et al.*⁶ and Luo *et al.*⁷ proposed to generate 3D molecules by employing the autoregressive model and flow-based model, respectively. The diffusion models have also been widely explored in molecule generation tasks⁸⁻¹⁰. Moreover, the Bayesian Flow Network¹¹ (BFN) is adopted to design unified generation pipelines of molecules^{12,13} and proteins^{14,15}, alleviating the differences between continuous and discrete data of molecules. These breakthroughs have greatly advanced the field of molecule generation, laying the groundwork for downstream applications and further research.

Although AI-driven technologies have demonstrated remarkable capabilities in generating molecular structures with diverse properties that promote the development of cutting-edge technologies like environmentally friendly chemicals^{5,16} and materials^{17,18}, these advancements also introduce significant challenges related to copyright and security, as the generated molecules fall outside the comprehensive regulatory frameworks. For example, unauthorized users potentially claim ownership of the generated molecules, which infringes on the copyright of the creators. Such misuse can lead to the proliferation of pirated molecular resources, exposing critical vulnerabilities in the protection of scientific innovation. Similar issues have emerged in the text and image generation models, where tools like ChatGPT can be used for academic dishonesty¹⁹, diffusion models²⁰⁻²² for creating fake images^{23,24}, and video generative models²⁵ for producing forged videos. These malicious activities pose serious security concerns and societal instability. In the context of molecule generation, the potential biopharmaceutical safety risks require strict regulation. As such, developing methods for embedding watermarking in molecules offers a promising pathway to safeguard intellectual property, prevent unauthorized replication, and ensure the trustworthy deployment of AI-generated molecular innovations²⁶.

However, protecting molecules is an emerging research topic in the field of information hiding. While copyright protection has been explored for traditional multimedia²⁷⁻³¹ and generated proteins^{32,33}, no dedicated methods have been developed for protecting molecules. The challenge of protecting molecules lies in the complexity of the task. Existing watermarking methods face compatibility problems when applied to molecules that are characterized by delicate and highly constrained architectures. Firstly, the finite number of atoms in a molecule imposes strict limitations on the available space for embedding watermarks. Secondly, molecular structures are highly sensitive to perturbations, and a slight change can disrupt atomic distances that break chemical bonds and render the molecules ineffective. Thirdly, watermarking methods must exhibit robustness to affine

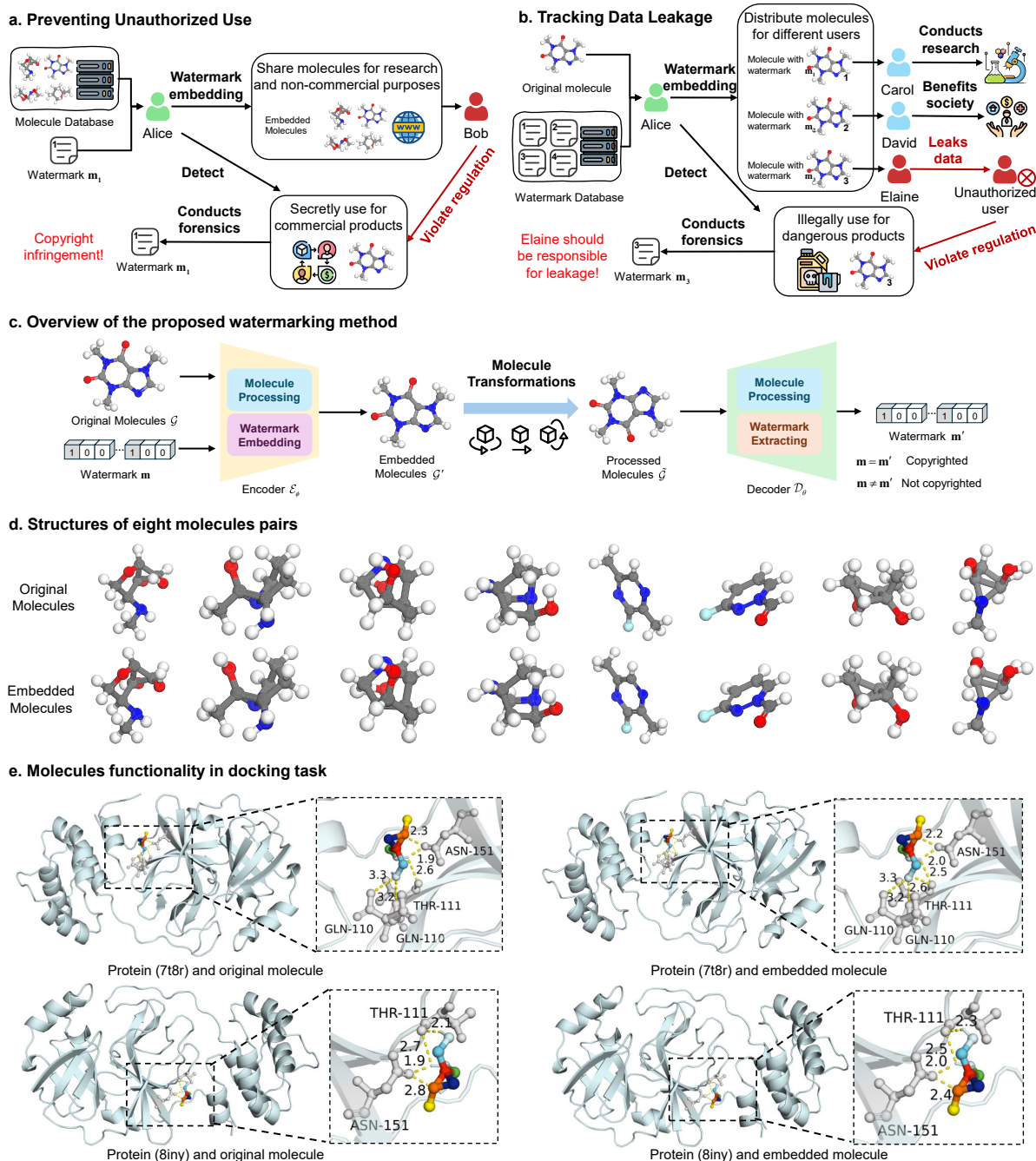


Figure 1. Application scenarios and performance of the proposed watermarking method in protecting molecules. a, Preventing unauthorized use. Alice embeds a specific watermark into molecules. Bob misuses them by violating the usage agreement, after which Alice detects the infringement and protects her copyright. **b,** Tracking data leakage. Alice distributes uniquely embedded molecules to different users. Elaine leaks her copy to unauthorized users, and Alice detects the leakage and successfully traces it back to Elaine. **c,** Overview of the proposed watermarking method. The encoder \mathcal{E}_ϕ embeds watermarks into molecules without compromising their properties, and the decoder \mathcal{D}_θ extracts the watermarks from molecules processed by transformations. **d,** Structure of eight pairs of molecules, in which the original molecule and embedded molecules are arranged vertically. The structure of the molecules only undergoes slight changes after watermark embedding. **e,** Effectiveness of the embedded molecules in the downstream task (molecule docking). For the original molecules and the embedded molecules, the amino acid residues and hydrogen bond lengths in molecular docking are similar, reflecting that the embedding watermark has an insignificant impact on the effectiveness of molecules.

transformations (*e.g.*, rotation, scaling, translation), as molecules retain their basic properties under such operations; however, most existing approaches remain vulnerable. These challenges highlight the pressing need for a robust watermarking framework specifically designed for molecular structures.

In this study, we propose the first AI-driven watermarking method designed specifically to safeguard the intellectual property of molecules. Initially, the encoder embeds the watermark into the structures of molecules, in which the node features are utilized to assist the embedding and maintain the molecular properties. Subsequently, the decoder extracts the watermark from the embedded molecules, providing copyright protection for molecules. To achieve robustness against affine transformations, we extract the invariant features for watermark embedding and extraction, after which the multidimensional scaling (MDS) strategy is utilized to solve the problem of numerical instability. During the training, we propose a dynamically balanced training strategy to optimize the proposed watermarking method, achieving the goal of copyright protection while maintaining the properties of molecules.

We comprehensively evaluate the proposed method through key performance analyses. **Preservation of molecular properties:** embedding a 16-bit watermark results in only a slight decrease in atom stability ($99.72\% \rightarrow 97.69\%$) and molecule stability ($95.00\% \rightarrow 94.60\%$), ensuring their suitability for subsequent scientific research. **Docking performance:** the embedded molecules retain strong binding ability, with the best binding affinity changing minimally ($-6.25 \text{ kcal/mol} \rightarrow -6.00 \text{ kcal/mol}$) and RMSD changing from 1.585 \AA to 1.602 \AA . **Robustness to transformations:** under affine transformations, the bit accuracies consistently exceed 95.00% . These results mark a significant step forward in molecular watermarking, offering a robust and reliable solution for safeguarding molecular intellectual property.

1 Results

To evaluate the performance of the proposed watermarking method, we utilize two benchmark datasets in molecular machine learning for comparison. The QM9 dataset³⁴ comprises approximately 134,000 molecules, each containing up to 29 atoms including hydrogens. The GEOM-DRUG dataset³⁵ includes 37 million conformations across roughly 450,000 drug-like molecules, offering a broader and more complex landscape with each molecule annotated with energy values and statistical weights. Both the QM9 dataset and the GEOM-DRUG dataset use the same partitioning method in previous studies^{8,36,37}, constructing the training, validation, and test sets with 100,000, 18,000, and 13,000 molecules, respectively. The generalization of the proposed watermarking method is evaluated by using two state-of-the-art unconditional generation models, GeoBFN¹² and GeoLDM⁸, which generate molecules to test the robustness and adaptability of the proposed watermarking method across diverse molecular landscapes.

We evaluate the performance of the proposed watermarking method through several experiments. Initially, we explore the feasibility of embedding watermarks into molecules without compromising the molecular properties. This foundational step confirms that the digital watermarks could be embedded into molecules effectively. Subsequently, we examine the impact of embedding different capacities of watermarks on molecular properties. Furthermore, we compare the performance of the proposed watermarking method with previous robust watermarking methods, revealing the necessity of proposing a new method instead of transferring existing methods for protecting molecules. The functionality of the embedded molecules is further analyzed, including the physicochemical properties and the docking performance in the downstream task. The robustness against affine transformations is evaluated by using the Special Euclidean group ($SE(3)$), which includes rotation, translation, and reflection. Finally, we perform ablation studies to dissect the contribution of different components within the proposed watermarking method. Through these analyses, we reveal the effectiveness of the proposed watermarking method on protecting molecules, providing insights for future refinement.

1.1 Feasibility of embedding watermarks into molecules

We first explore the feasibility of embedding watermarking into molecules. Mathematically, the watermark \mathbf{m} is defined as a binary sequence with length L , allowing for 2^L unique watermarks to be embedded into molecules. While embedding watermarks has been successfully applied to domains like images and proteins, directly transferring these techniques to molecules introduces a fundamental mismatch. To illustrate this, Table 1 compares the structural characteristics of images, proteins, and molecules. Specifically, images are composed of discrete pixels, offering high redundancy and low sensitivity to modification. The proteins are relatively more complex, containing non-critical regions and exhibiting moderate sensitivity. In contrast, molecules are constructed by strict chemical constraints, rendering structures highly sensitive to slight perturbation. In the aspect of embedding capacity, pioneering watermarking methods^{27,28,31} embed 30 bits into images sized $128 \times 128 \times 3$, yielding a bit per pixel (BPP) ratio of approximately 1.83×10^{-3} . Meanwhile, 32 bits of watermark are embedded into proteins with 500×37 atoms³², resulting in a bit per atom (BPA) of about 1.73×10^{-3} . For molecules in datasets like QM9 and GEOM-DRUG, no more than 200 atoms are contained in one molecule. Considering the structural characteristics of molecules, embedding watermarks for copyright protection is a highly challenging task.

Table 1. Comparative analysis of the difference between images, proteins, and molecules.

	Images	Proteins	Molecules
Dimension	2D/3D	3D	3D
Structure	Discrete pixels	Multimodal data	Multimodal data
Property	High redundancy	Non-critical regions	Strict chemical constraints
Sensitivity	Low	Moderate	High
Space	High (128×128×3 pixels)	Moderate (500×37 atoms)	Extremely low (200 atoms)

At the same embedding rate (i.e., BPA) observed in protein protection³², the theoretical watermark length for molecules is $L = 0.35$ bits. Given that the watermark length must be an integer, we set $L = 1$ to explore the feasibility of embedding a watermark into molecules, in which the 1-bit watermark carries significant utility for verifying authenticity, detecting tampering, and confirming whether a molecule originates from a legitimate source. The basic properties of the embedded molecules and the extractability of the watermark are adopted as the evaluation metrics, which are measured in percentages (%). Specifically, the basic properties in the prior works^{8,12,37,38} include atom stability (Atom Sta), molecule stability (Mol Sta), validity, uniqueness (Uniq), and novelty. The atom stability assesses the correctness of atom positions by examining the rationality of chemical bonds, and the molecule stability measures the overall structural coherence of the molecules. Furthermore, the validity determines whether the molecular structure adheres to fundamental chemical rules. The uniqueness decides whether two molecules are structurally identical, and the novelty evaluates whether the molecules exist in benchmark datasets. Meanwhile, the extractability of the watermark is reflected by the bit accuracy (Bit Acc), referring to the proportion of correctly extracted bits relative to the total embedded bits. Leveraging these evaluation metrics, the feasibility of embedding watermarks into molecules depends on maintaining the basic properties of molecules and improving the bit accuracy. From a quantitative perspective, higher values of these metrics indicate better performance and feasibility.

Fig. 2 (a) shows the results of embedding a 1-bit watermark into the molecules from the QM9 and GEOM-DRUG datasets. For the molecules in the QM9 dataset, the basic properties exhibit high numerical values, in which the atom stability, molecule stability, and validity are 99.00%, 95.20%, and 97.70%, respectively. After embedding a watermark, these properties remain largely intact, in which the atom stability, molecule stability, and validity are 98.41%, 95.00%, and 97.54%, respectively. The bit accuracy is 99.69%, indicating that the embedded watermark can be extracted accurately. For the molecules in the GEOM-DRUG dataset, the basic properties decrease slightly. For example, atom stability decreases from 86.50% to 86.12%, and the validity decreases from 99.90% to 92.08%. Meanwhile, the bit accuracy is 99.82%, demonstrating the feasibility of embedding watermarks in molecules.

Furthermore, Fig. 1 (d) presents eight pairs of molecular structures, in which each original molecule is alongside its watermarked counterpart. The visual differences between the original and watermarked molecules are minimal, with core structures remaining intact. In addition, only slight deviations are observed in the positions of hydrogen atoms, while the changes in the positions of non-hydrogen atoms can be ignored. According to the results mentioned above, we demonstrated that it is feasible to embed watermarks into molecules, in which the basic properties can be preserved and the embedded watermark can be reliably extracted.

1.2 Impacts of different embedding capacity on molecular structures

Our previous results have confirmed the feasibility of embedding a 1-bit watermark into molecules by using the proposed watermarking method. However, the minimal capacity limits the practical applications and requires further improvement in embedding capacity. Generally, increasing the watermark capacity typically introduces greater structural perturbation. To investigate this impact, we set the embedding capacity L from 4 bits to 16 bits, achieving a balance between the need for copyright protection and the preservation of molecular properties.

Fig. 2 (a) presents the impact of different embedding capacities of watermark on molecules generated by the model GeoBFN. Compared to the original molecules, embedding watermarks has a slight impact on the basic properties of molecules. To illustrate, consider the embedding capacity of 8 bits. The atom stability of the original molecules is 99.72%, while that of the watermarked molecules is 98.06%. Similarly, the molecule stability shows a modest decline from 95.00% to 94.68%. Other properties of the original molecules and the embedded molecules are similar, such as the validity (97.65% and 97.45%) and uniqueness (85.22% and 85.20%), indicating that our proposed method for embedding watermarks can effectively preserve the structural integrity. The novelty increases from 72.99% to 73.07%, suggesting that the subtle perturbations introduced by embedding watermarks enhance structural diversity and lead to more innovative molecular conformations. On the premise of ensuring basic properties, the bit accuracy is 95.59%, affirming that the watermark remains reliably extractable.

As the embedding capacities increase, the basic properties present a slight decline. Notably, atom stability remains

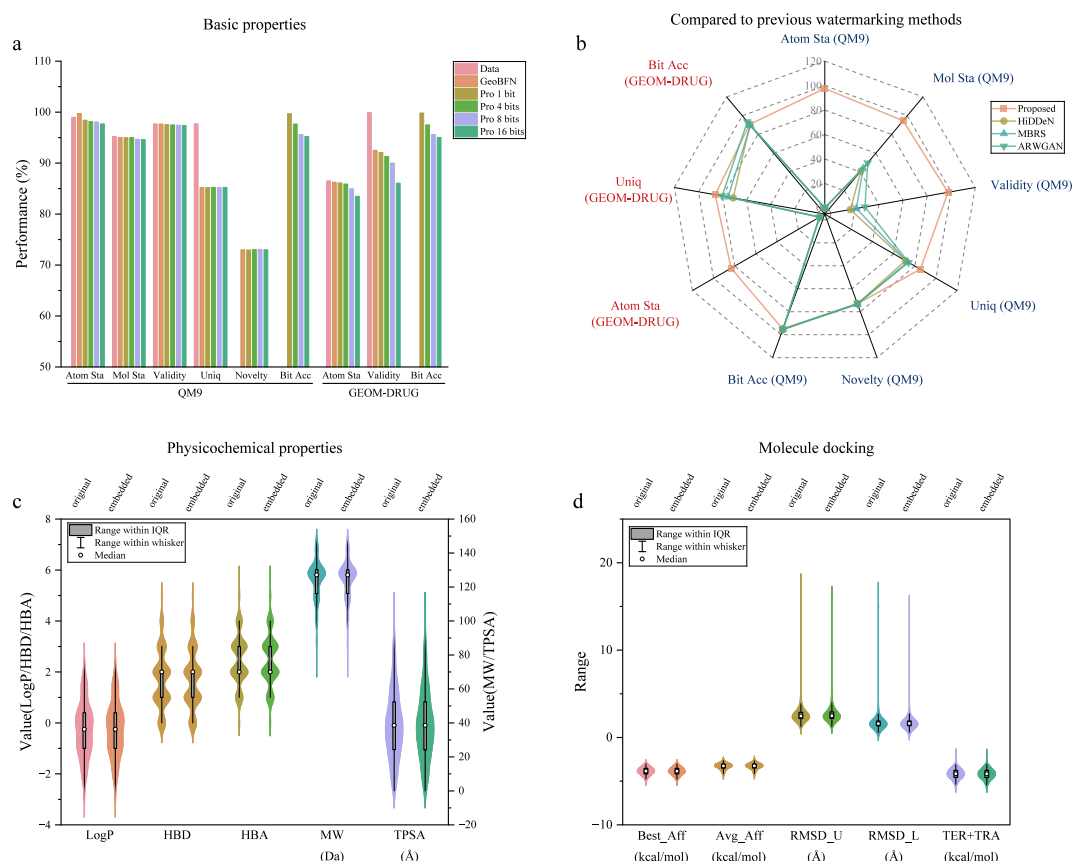


Figure 2. Impact of embedding watermark on molecules. **a**, Impacts of different embedding capacity on molecular basic properties. The molecules are generated by GeoBFN, which is trained on QM9 and GEOM-DRUG datasets, respectively. **b**, Comparison to the previous watermarking methods. The proposed watermarking method can protect the molecules and maintain the basic properties, while the previous watermarking methods disrupt the structure of molecules. **c**, Impact of embedding watermark on the physicochemical properties of molecules, in which the distributions of embedded molecules are close to that of the original molecules. **d**, Impact of embedding watermark on molecule docking downstream task, in which the docking results of embedded molecules are close to those of the original molecules.

consistently at high values, exceeding 97.69% at a capacity of 16 bits. In addition, the molecule stability, validity, and uniqueness are 94.60%, 97.36%, and 85.21%, respectively, indicating that the structures of the molecules remain largely intact. Importantly, the bit accuracy remains higher than 95.20%, demonstrating that the watermark can still be reliably extracted even when more information is embedded. Overall, these results highlight the generalization of the proposed watermarking method across different molecular structures, making it a promising tool for safeguarding molecular data. Additional results on molecules generated by GeoLDM⁸ are provided in Supplementary Section 1.1.

The experimental results across different embedding capacities demonstrate that the proposed watermarking method can effectively protect molecules while preserving the basic properties. The balance between bit accuracy and molecular properties enables copyright protection and content traceability. As generative models become more prevalent in molecular design, such watermarking strategies offer a promising path toward secure, transparent, and ethically governed molecular innovation.

1.3 Compared to previous watermarking methods on molecule protection

In the literature, deep learning based watermarking methods have been extensively explored for traditional multimedia, including images, audio, and video. Zhu *et al.*²⁷ proposed HiDDeN, an encoder-noise layer-decoder architecture, in which the encoder embeds the watermark, the decoder extracts the embedded watermark, and the noise layer enhances resilience against differentiable attacks such as additive noise and pixel cropping. To address non-differentiable attacks like real JPEG compression, a two-stage framework²⁸ and mini-batch strategy (MBRS)²⁹ are proposed to improve robustness. Fang *et al.*³⁰ pointed out that the encoder-decoder structure may produce redundant or irrelevant features, and proposed a decoder-driven approach that improves feature coupling and reduces redundancy. Huang *et al.*³¹ proposed ARWGAN, which further advances

robustness by integrating attention mechanisms and generative adversarial networks. These watermarking methods strengthen copyright protection for multimedia files, representing significant technological advancements.

Though existing watermarking methods have achieved great robustness in protecting multimedia files, directly applying these methods to protect molecules leads to mismatch problems. To alleviate these problems, we modify the source codes in HiDDeN²⁷, MBRS²⁹, and ARWGAN³¹ to fit the embedding of watermark on molecules, after which the QM9 and GEOM-DRUG datasets are used for training. The model GeoBFN is then utilized to generate molecules, and the embedding capacity is set to 16 bits. Fig. 2 (b) presents the performance of the proposed watermarking method and the previous watermarking methods on protecting molecules. The basic properties of molecules and the bit accuracy are adopted as evaluation metrics. For the models trained on the QM9 dataset, the bit accuracies of the proposed watermarking method, HiDDeN, MBRS, and ARWGAN are 95.20%, 94.64%, 95.34%, and 95.45%, respectively. Though the bit accuracies are comparable, previous watermarking methods significantly compromise molecular properties. For instance, the molecular stability of HiDDeN, MBRS, and ARWGAN all decrease to 0.00%, and the atom stability declines to 40.95%, 43.75%, and 49.61%, respectively. Additionally, the novelty, validity, and uniqueness fall to approximately 70.00%, suggesting that the functionality of these embedded molecules tends to be ineffective. In contrast, the proposed watermarking method consistently maintains the basic properties around 90.00%, underscoring the effectiveness in safeguarding molecular properties after embedding watermarks.

Experimental results highlight the structural damage caused by previous watermarking methods, demonstrating their inability to be directly applied to molecular protection. In contrast, the proposed watermarking method achieves a balance between bit accuracy and molecular properties, enabling copyright protection and content traceability for molecules. As generative models become more prevalent in molecular design, the proposed watermarking method offers a promising path toward secure, transparent, and ethically governed molecular innovation.

1.4 Analysis of the physicochemical properties of molecules

In addition to the basic properties, we analyze the impact of embedding watermarks on the physicochemical properties of molecules. The structural rationality is first evaluated by using RDKit³⁹ and the OpenBabel⁴⁰, which check for the fundamental chemical rules including chemical bonds, stereochemistry, and ring tension, etc. After that, those molecules with reasonable structures are further validated the physicochemical properties by using the RDKit and the MDAnalysis^{41,42}, in which the key metrics include lipid water partition coefficient (LogP), hydrogen bond donor (HBD), hydrogen bond acceptor (HBA), molecular weight (MW), and topological polar surface area (TPSA). The LogP reflects the lipophilicity of the molecules, in which $\text{LogP} > 0$ indicates the molecules have strong lipophilicity that are more soluble in lipid environments, while $\text{LogP} < 0$ means the molecules have strong hydrophilicity that are more soluble in aqueous phases. The HBD refers to the number of donor groups that can form hydrogen bonds, and HBA is the number of acceptor atoms that can form hydrogen bonds. The MW is the sum of the atomic weights within a molecule, measured in Dalton (Da) or g/mol. Based on Ertl's algorithm⁴³, TSPA calculates the total projected area of polar atoms on the molecular surface. Leveraging these metrics for evaluation, the impact of embedding watermarks on the physicochemical properties of molecules can be reflected in a comprehensive view. Detailed definitions and additional descriptions are available in Supplementary Section 1.2.

The tested molecules are generated by using the model GeoBFN, after which the proposed watermarking method embeds 8 bits of watermarks into molecules. The structural analysis has revealed that about 97.50% of the original molecules and 95.30% of the embedded molecules remain chemically valid. The primary reason for molecular invalidity is that the carbon atoms exceed their valence limits. For those valid molecules, Fig. 2 (c) illustrates the distribution of the physicochemical properties, which are calculated from the original molecules and the embedded molecules. We describe these distributions statistically, including the median, the interquartile range (IQR), and the whisker length. The median represents the center of the distribution and is not affected by extreme values, making it more representative of typical values than the average. The IQR measures the degree of dispersion in the middle 50% of the distribution, and we present IQR with the first quartile (Q1) and third quartile (Q3) in the format of "IQR (Q1 to Q3)" to better illustrate the range. The larger the IQR, the more dispersed the intermediate data. The whisker length is determined by the range between the upper and lower edges of the distribution, with these edges serving as the truncation points for outliers. We present whisker in the format of "Whisker (lower edge to upper edge)", where a larger whisker indicates greater dispersion within the distribution. Therefore, the small values of IQR and whisker indicate a highly concentrated data distribution.

The original molecules and the embedded molecules have the same median LogP of -0.25, with the IQR of 1.40 (-1.00 to 0.4) and whisker of 5.50 (-3.06 to 2.44), indicating that embedding a watermark maintains the lipophilic and hydrophilic characteristics of molecules. The medians of HBD are 2.00 for the original molecules and the embedded molecules, with the same IQRs of 1.00 (1.00 to 2.00) and whiskers of 3.00 (0.00 to 3.00). Meanwhile, the medians of HBA for the original molecules and the embedded molecules are 2.00, with the same IQRs of 1.00 (2.00 to 3.00) and whiskers of 3.00 (1.00 to 4.00). The similar distributions of HBD and HBA support that embedding a watermark ensures consistency of functional groups within the molecules. Furthermore, the MW of the original and embedded molecules centers at 127.14 Da, with

the same IQRs of 14.02 Da (116.17 Da to 130.19 Da) and whiskers of 53.08 Da (96.11 Da to 149.19 Da), suggesting high penetrability. The TPSA has a median of 38.55 Å² for both the original and embedded molecules, with the same IQRs of 28.22 Å² (24.27 Å² to 52.49 Å²) and whiskers of 90.52 Å² (3.01 Å² to 93.53 Å²), supporting good membrane permeability. These similar distributions confirm that embedding a watermark maintains the physicochemical properties of molecules and ensures independence from subsequent scientific research. Additionally, the low MW of embedded molecules contributes to the high penetrability, promoting applications in downstream tasks. Detailed analysis of the physicochemical properties across different embedding capacities of the watermark is available in Supplementary Section 1.2.

1.5 Impact on downstream task: molecule docking

To evaluate the impact of embedding watermarks on subsequent scientific research of molecules, we conduct molecule docking as the downstream task. We first generate 100 molecules using the model GeoBFN. After that, the proposed watermarking method embeds 8 bits of watermark to generate the embedded molecules. In this way, the ligands for molecule docking include 100 original molecules and 100 embedded molecules. For the receptors, we select 50 proteins from the RCSB Protein Data Bank⁴⁴ (RCSB PDB), in which the PDB accession codes (PDB ID) are listed in Supplementary Section 1.3. The docking simulations are performed by using the widely adopted tool AutoDock Vina^{45,46}, which is known for the accuracy and efficiency in predicting ligand-receptor interactions. In this way, we evaluate whether the embedded molecules still engage meaningfully with biological targets as the original ones, offering insight into the applicability of embedding watermarks in molecular design and drug discovery.

The performance of molecule docking is evaluated by utilizing the binding affinity (Aff), the root mean square deviation (RMSD), the interaction energy (INTER) between receptors and ligands, and the internal energy of ligands (INTRA) as the metrics. Lower values across these evaluation metrics indicate better docking performance. Fig. 2 (d) illustrates the distribution of the docking results between proteins and molecules, in which the results of original molecules and embedded molecules are listed in parallel. We analyze these distributions statistically, including the median, IQR, and whisker length. For the best binding affinity (Best_Aff), the medians of original molecules and embedded molecules are -3.86 kcal/mol and -3.85 kcal/mol, respectively. The original molecules exhibit an IQR of 0.63 kcal/mol (-4.17 kcal/mol to -3.54 kcal/mol) with a whisker of 2.51 kcal/mol (-5.12 kcal/mol to -2.61 kcal/mol). Meanwhile, the embedded molecules show a comparable distribution, with an IQR of 0.64 kcal/mol (-4.17 kcal/mol to -3.53 kcal/mol) and a whisker of 2.52 kcal/mol (-5.13 kcal/mol to -2.61 kcal/mol). These closely aligned distributions indicate that the embedded molecules generally preserve docking functionality. The RMSD reveals the conformational deviations. For the upper bound of the RMSD (RMSD_U), the medians of original molecules and embedded molecules are 2.46 Å and 2.47 Å respectively, with the IQRs of 0.71 Å (2.17 Å to 2.88 Å) and 0.75 Å (2.18 Å to 2.93 Å), and whiskers of 2.74 Å (1.19 Å to 3.93 Å) and 2.96 Å (1.08 Å to 4.04 Å). Additionally, the binding energies (INTER+INTRA) of the original and the embedded molecules are similar, in which the medians are both -4.16 kcal/mol, with IQRs of 0.81 kcal/mol (-4.57 kcal/mol to -3.76 kcal/mol) and 0.81 kcal/mol (-4.67 kcal/mol to -3.86 kcal/mol), and whiskers of 3.26 kcal/mol (-5.80 kcal/mol to -2.54 kcal/mol) and 3.27 kcal/mol (-5.80 kcal/mol to -2.53 kcal/mol). Collectively, the docking results demonstrate that the embedded molecules retain docking efficacy comparable to the original molecules, underscoring the feasibility of the proposed watermarking method in molecular interaction contexts.

Fig. 1 (e) presents four docking renderings, in which the original molecule, the embedded molecule, and two proteins with PDB IDs of 7t8r and 8iny are utilized for docking experiments. Across these examples, the hydrogen bond lengths and the amino acid residues are notably similar between the two molecules. For the protein 7t8r, the binding affinities of the original and embedded molecules are -5.80 kcal/mol and -5.79 kcal/mol, respectively. Similarly, for protein 8iny, the binding affinities are -5.90 kcal/mol for the original molecule and -5.83 kcal/mol for the embedded molecule. Overall, the docking results demonstrate that both original and embedded molecules exhibit stable binding affinities and the same conformations when interacting with proteins, affirming that embedding watermark maintains the functionality of molecules in downstream applications. More details of molecule docking are available in Supplementary Section 1.3.

1.6 Robustness against SE(3) transformations

The robustness of the proposed watermarking method is evaluated by using the SE(3) transformations, which include rotation, translation, and reflection. Initially, we generate the molecules by using the model GeoBFN, after which the proposed watermarking method embeds watermarks ranging from 4 bits to 16 bits. Subsequently, the embedded molecules are processed by SE(3) transformations to simulate real-world perturbations. Finally, the embedded watermarks are extracted from the processed molecules to calculate the bit accuracy, which is utilized as the evaluation metric for robustness comparison. The bit accuracy is a direct reflection of the robustness, ensuring reliable copyright protection for molecules.

1.6.1 Robustness against rotation

Fig. 3 (a) presents the result of the original molecule rotating clockwise 90 degrees on the X axis, in which the rotated molecule has the same properties but a different conformation. Fig. 3 (b) illustrates the distribution of bit accuracy across different

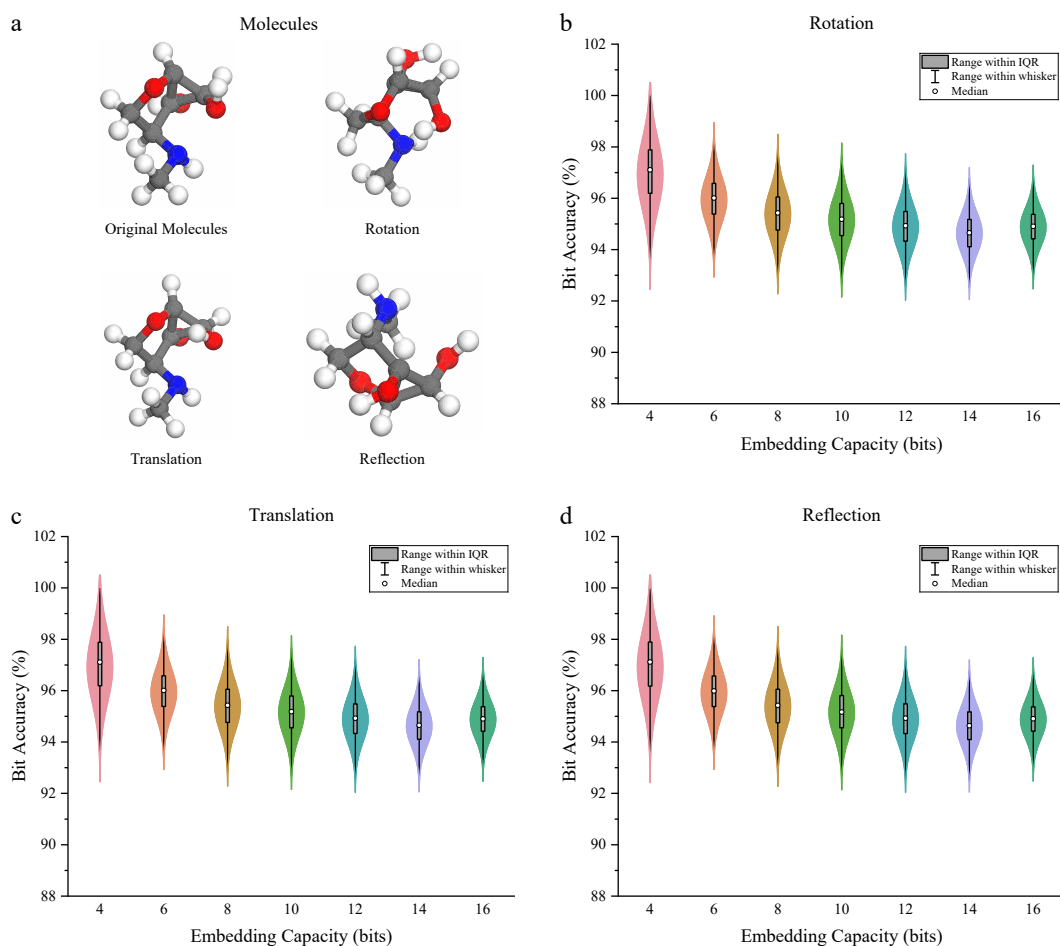


Figure 3. Robustness against SE(3) transformations. **a**, The confirmations of molecule after applying SE(3) transformations, including rotation, translation, and reflection. The conformations of the processed molecules are different, but they share the same characteristics. **b**, Bit accuracy against rotation under different watermark capacities. **c**, Bit accuracy against translation under different watermark capacities. **d**, Bit accuracy against reflection under different watermark capacities.

embedding capacities, in which the rotation is performed along the X, Y, and Z axes. The rotation angle α ranges from 0 to 360 degrees in increments of 10 degrees. We describe the distributions of bit accuracy with the median, IQR, and whisker length. For example, consider the embedding capacity of 8 bits. The median of bit accuracy is 95.43%, with the IQR of 1.29% (94.76% to 96.05%) and the whisker of 5.15% (92.83% to 97.98%). At the higher capacity of 16 bits, the median of bit accuracy decreases to 94.90%, with an IQR of 0.95% (94.42% to 95.37%), and the whisker of 3.82% (92.99% to 96.81%). Across different embedding capacities and rotation angles, the medians of bit accuracy are consistently higher than 94.65%, demonstrating the strong robustness of the proposed watermarking method against rotation. Therefore, the robustness ensures that embedded watermarks remain reliably extractable, even when molecular orientations vary significantly.

Specifically, the bit accuracy for each molecule remains identical across different rotation angles for each embedding capacity. This consistency highlights the robustness of the proposed watermarking method in resisting rotation. On the premise of maintaining the molecular properties, the bit accuracy gradually decreases as the embedding capacity increases. In this way, the balance between the bit accuracy and the molecular properties can be achieved, which is a necessary compromise to preserve the structural and functional effectiveness of molecules. Despite these constraints, the proposed watermarking method consistently achieves high bit accuracy across different rotation operations. More details of the robustness against rotation are available in Supplementary Section 1.4.1.

1.6.2 Robustness against translation

Fig. 3 (a) presents the result of translating the original molecule by 0.5 on the X axis, in which the translated molecule has the same properties and conformation. We apply the translation along the X, Y, and Z axes, in which the translation value ranges from -1.8 to 1.8 in an interval of 0.1. Fig. 3 (c) illustrates the distribution of bit accuracy across different embedding capacities.

We describe the robustness in a statistical way, including the median, IQR, and whisker length. At an embedding capacity of 8 bits, the median bit accuracy is 95.43%, with the IQR of 1.29% (94.76% to 96.05%), and the whisker of 5.17% (92.82% to 97.99%), showing occasional deviations but overall strong robustness. As the embedding capacities increase, a gradual decline in bit accuracy is observed. Nevertheless, all the medians of bit accuracy remain above 94.65% across different embedding capacities, confirming the robustness of the proposed watermarking method against translation.

For each molecule, the bit accuracy remains consistent across different translation values under the constraint of the same embedding capacity. This consistency highlights the robustness of the proposed watermarking method in resisting translation. However, maintaining molecular properties imposes constraints on embedding watermarks into molecules, leading to the slight fluctuation of bit accuracy across different molecules and embedding capacities. Overall, the proposed watermarking method can consistently achieve bit accuracies higher than 95.00% under these constraints, demonstrating stable performance. Additional results of robustness against translation are available in Supplementary Section 1.4.2.

1.6.3 Robustness against reflection

Fig. 3 (a) presents the result of reflecting the original molecule on the X axis, in which the processed molecule has the same properties but a different conformation. We apply the reflection on the X, Y, and Z axes. Fig. 3 (d) presents the distribution of bit accuracies under different embedding capacities, in which the reflection simulates the mirrored molecular operation to test the robustness of the proposed watermarking method.

We analyze the distribution of bit accuracy in a statistical way, including the median, IQR, and whisker length. At an embedding capacity of 8 bits, the median of bit accuracy is 95.43%, with the IQR of 1.31% (94.75% to 96.06%), and the whisker of 5.20% (92.80% to 98.00%), indicating high consistency across most molecules. For the embedding capacity of 16 bits, the median of bit accuracy is 94.90% and the IQR of 0.95% (94.42% to 95.37%). Meanwhile, the whisker is 3.75% (93.03% to 96.78%), reflecting stable central clustering. As the embedding capacity increases, the bit accuracy gradually decreases but remains within a high-value range. The results of bit accuracy have shown that the proposed watermarking method is robust against reflection under different embedding capacities. Across different reflection axes, the proposed watermarking method can achieve high bit accuracies, protecting the molecules with stable robustness. More details of the robustness against translation are available in Supplementary Section 1.4.3.

As illustrated in Fig. 3 (b) to (d), the proposed watermarking method exhibits strong robustness against SE(3) transformations, including rotation, translation, and reflection. The robustness originates from the utilization of SE(3) invariant features, as introduced in Section 3. By leveraging the invariant features, the embedded watermarks remain stable and extractable after processing the embedded molecules. Therefore, the proposed watermarking method not only preserves molecular properties but also provides a reliable mechanism for copyright protection, enabling secure and traceable molecule protection.

1.7 Effectiveness of model structure using ablation studies

The proposed watermarking method is an AI-driven model with a delicate architectural design, which achieves copyright protection without compromising the molecular properties. As shown in Section 3.1.1, the key components of the proposed model are the *atom embedder* and the *edge embedder*, in which the effectiveness of these two components is assessed by conducting comprehensive ablation studies. Three variant models of the original model are constructed for comparison, in which Variant1 removes the atom embedder, Variant2 removes the edge embedder, and Variant3 removes both the atom embedder and the edge embedder. For consistency, the QM9 and GEOM-DRUG datasets are utilized to train all variant models under an embedding capacity of 10 bits. The basic properties of molecules and the bit accuracy of extracted watermarks are utilized as evaluation metrics.

The model GeoBFN is utilized to generate molecules for comparisons. Fig. 4 (a) presents the comparative analysis of the original model and the three variant models. Among the four compared models, the original model consistently outperforms the three variant models in maintaining the basic properties of molecules. Focusing on atom stability and molecule stability, the Variant1 performs better than Variant2, suggesting that keeping the edge embedder can improve the stability. Such an advantage originates from the use of atom distances, which constrain the distortions caused by embedding watermarks. Without the assistance of the atom embedder and edge embedder, Variant3 exhibits the worst performance among the variant models. Considering the results in Fig. 4 (a), we demonstrate that both the atom embedder and the edge embedder are beneficial for embedding a watermark into molecules, contributing to maintaining the properties of molecules.

To further evaluate the robustness of the original model and the three variant models, the SE(3) transformations are applied to modify the embedded molecules. Fig. 4 (b), (c), and (d) present the distributions of bit accuracy calculated from molecules processed by rotation, translation, and reflection, respectively. We analyze the distribution in statistical ways, including the median, IQR, and whisker length. In general, the median of bit accuracy gradually decreases from the original model to Variant1, Variant2, and finally Variant3. For example, under the rotation operation, Variant1 achieves a median bit accuracy of 93.75%, with an IQR of 1.56% (92.97% to 94.53%), and whisker of 6.09% (90.63% to 96.72%). Meanwhile, the medians of Variant2 and Variant3 are 93.13% and 92.97%, respectively. Among the three variant models, Variant1 consistently demonstrates the highest

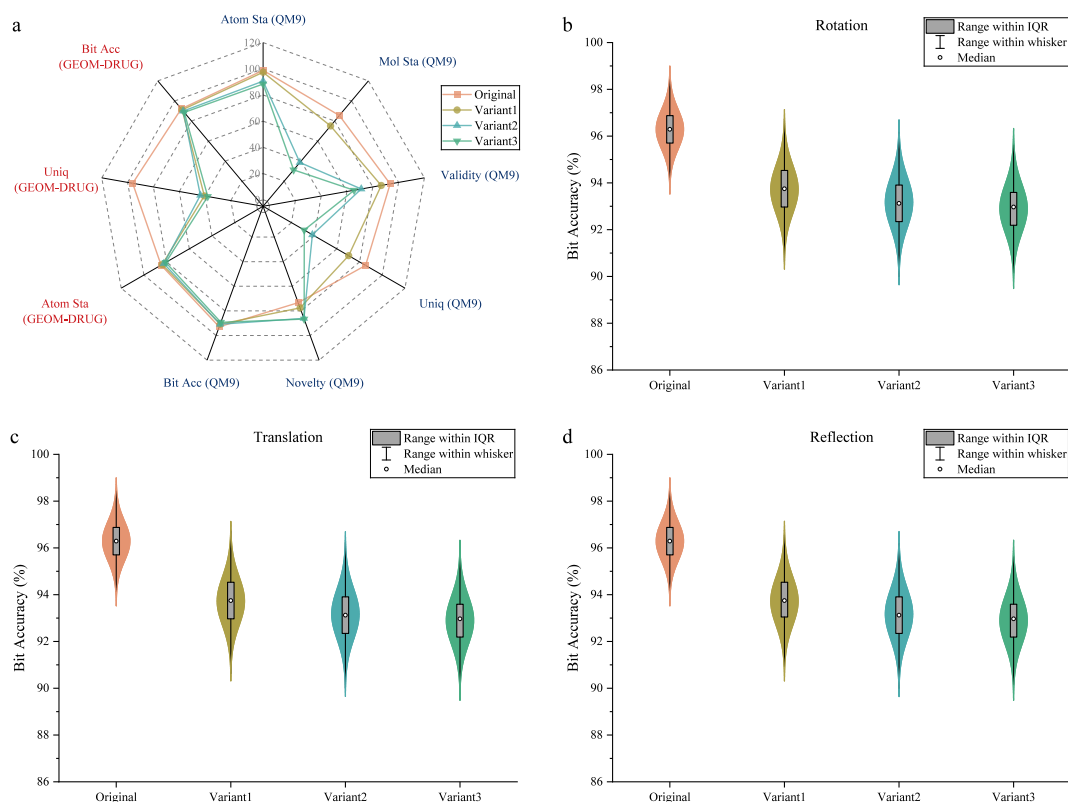


Figure 4. Effectiveness of model structure using ablation studies. **a**, The basic properties of molecules after embedding 10 bits by the original model and the three variants. **b**, Bit accuracy of the original model and the three variants against rotation. **c**, Bit accuracy of the original model and the three variants against translation. **d**, Bit accuracy of the original model and the three variants against reflection.

robustness, followed by the Variant2 and Variant3. Notably, the original model and three variant models maintain median bit accuracies above 92.97%, underscoring the robustness of the proposed watermarking method against SE(3) transformations.

In conclusion, these findings highlight that the integration of the atom embedder and edge embedder significantly enhances the performance of the proposed watermarking method, contributing to maintaining the molecular properties and enhancing robustness against SE(3) transformations. In addition, a delicate design contributes to improving the performance of the copyright protection method, which is worth further exploration.

2 Discussion

In this study, we propose the first watermarking method for molecules, which utilizes an AI-driven model to protect copyright and trace leakage. In the watermark embedding process, the atom features and edge features are considered to minimize the structural perturbations, effectively maintaining the molecular properties. The robustness against SE(3) transformations (rotation, translation, and reflection) is achieved by utilizing the SE(3) invariant features, which originate from the Euclidean distance between atoms. Leveraging the MDS method, the invariant features are projected into the low-dimensional representation, solving the issue of data instability and improving the watermark extraction accuracy. Comprehensive experiments are conducted to evaluate the impact of embedding watermarks on molecules, revealing that the proposed watermarking method achieves high bit accuracy without compromising the properties of molecules. Additionally, the molecule docking results have verified that the embedded molecules have functionality similar to that of the original molecules in the downstream task. Furthermore, the proposed watermarking method exhibits strong robustness against SE(3) transformations. These findings highlight the potential of the proposed watermarking method as a novel and effective strategy for molecule protection, enabling the prevention of unauthorized use and traceability of data leakage.

The challenge of preserving the structural and functional integrity of molecules during watermark embedding presents a significant impediment in the field of molecule protection. Experimental results have shown that the proposed watermarking method embeds watermarks into molecules with minimal perturbation to molecular structures, which is reflected in maintaining

the properties and functionality in downstream tasks. However, embedding watermarks may modify the molecular interactions, potentially impacting the efficacy in pharmaceutical and biological research. Therefore, further evaluation of the functional properties of embedded molecules is necessary, encompassing aspects such as biological activity, chemical reactivity, and physical behavior.

Furthermore, the challenge of editing molecules on the robustness of watermarking methods is focused on extracting watermarks accurately from the processed molecules. In this study, the proposed watermarking method achieves robustness against SE(3) transformations, in which the molecules are processed without changing the structures. However, other molecular editing techniques, such as clipping or structural folding, can significantly disrupt the molecular structures, raising controversy about copyright ownership of these processed molecules and challenges for the robustness of the watermarking method. As such, enhancing robustness against non-destructive yet structurally impactful modifications remains a promising direction. Strengthening watermark robustness under such conditions will be crucial for ensuring the protection of molecules in both scientific and commercial applications.

The robustness of the proposed watermarking method is essential for defending against infringement, but it comes at the cost of permanent structural distortion to molecules. Although effective for anti-counterfeiting, the irreversible modifications impede the use of embedded molecules in critical downstream applications, such as drug discovery, catalysis, or biological studies. Our vision for molecule watermarking is to achieve robustness without sacrificing the original molecular structures, ensuring that embedded molecules can be restored to the original structures without loss. Traditionally, watermarking methods prioritize robustness over reversibility, and our vision challenges the conventional paradigm of watermarking methods. By considering both robustness and reversibility, this outlook opens new possibilities for secure yet scientifically viable molecule protection.

3 Methods

In this study, we propose the first universal watermarking method tailored for molecule protection. The proposed watermarking method embeds a watermark into molecules with a slight impact on molecular properties while achieving strong robustness against SE(3) transformations such as rotation, translation, and reflection. Fig. 1 (a) and (b) illustrate the application scenarios of the proposed watermarking method, including preventing unauthorized use and tracking data leakage. The proposed watermarking method offers a powerful tool for safeguarding molecules.

In the scenario of preventing unauthorized use in Fig. 1 (a), Alice embeds a specific watermark \mathbf{m}_1 into the molecule database before sharing for research and non-commercial use. However, Bob violates the regulation and secretly employs the molecules in commercial products. Upon detecting suspicious activity, Alice conducts a forensic analysis and extracts watermark \mathbf{m}_1 from the unauthorized products. This confirms the infringement and enables Alice to assert her copyright, thereby reinforcing accountability. In the scenario of tracking data leakage in Fig. 1 (b), Alice embeds different watermarks into molecules, generating exclusive molecules for different users. Carol and David use their versions responsibly for scientific research and social benefit, while Elaine leaks her copy to unauthorized users, who may exploit the molecules for illicit or hazardous purposes. Through forensic tracing, Alice identifies watermark \mathbf{m}_3 in the leaked samples, linking the source of the leak to Elaine. In this way, Alice can pinpoint the source of the leak and hold the responsible party accountable. These scenarios reflect that the proposed watermarking method can safeguard intellectual property, enforce usage policies, and trace unauthorized distribution while preserving the scientific utility of the molecules.

Fig. 1 (c) shows the overview of the proposed watermarking method, consisting of the watermark encoder \mathcal{E}_ϕ and decoder \mathcal{D}_θ . Initially, the encoder \mathcal{E}_ϕ embeds the watermark into the structures of the molecules without compromising the molecular properties. Subsequently, molecule transformations (rotation, translation, and reflection) are applied to modify the embedded molecules, simulating the commonly used post-processing. Finally, the decoder \mathcal{D}_θ extracts the watermark from the embedded molecules, achieving the goal of copyright protection for molecules. The entire framework is implemented as a trainable deep learning model, allowing performance optimization through end-to-end training. The processes of embedding and extracting watermarks are described as follows.

3.1 Watermark Embedding

The encoder \mathcal{E}_ϕ is designed to embed watermarks into molecules while preserving the molecular properties. Let d denotes the dimension of node features, and N represents the number of atoms in a molecule. Each 3D molecule can be represented as the geometry $\mathcal{G} = (\mathbf{p}, \mathbf{h}) \in \mathbf{R}^{N \times (3+d)}$, in which $\mathbf{p} = (\mathbf{p}_1, \dots, \mathbf{p}_N) \in \mathbf{R}^{N \times 3}$ is the atom positions and $\mathbf{h} = (\mathbf{h}_1, \dots, \mathbf{h}_N) \in \mathbf{R}^{N \times d}$ denotes the node features. The node features \mathbf{h} are composed of the atom type $\mathbf{t} = (\mathbf{t}_1, \dots, \mathbf{t}_N) \in \mathbf{R}^{N \times e}$, the atom charge $\mathbf{c} = (\mathbf{c}_1, \dots, \mathbf{c}_N) \in \mathbf{R}^{N \times 1}$, and the edge indexes $\mathbf{e} = (\mathbf{e}_1, \dots, \mathbf{e}_N) \in \mathbf{R}^{N \times (N-1)}$. Specifically, the atom types are encoded as one-hot vectors, where e represents the number of atomic species in the dataset. In the QM9 dataset, e is 5, while in the GEOM-DRUG dataset, e is 16.

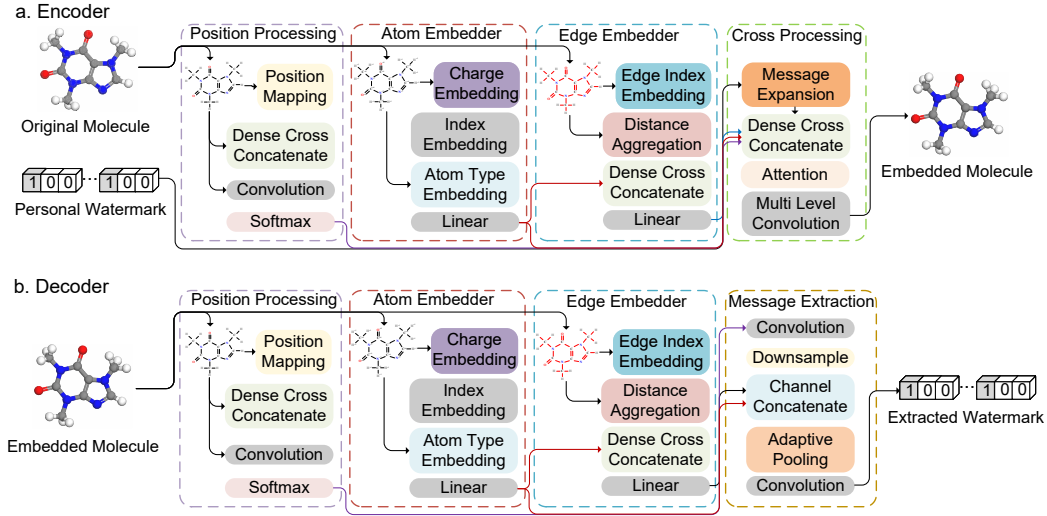


Figure 5. The structures of the proposed watermarking method. **a** The structure of the encoder \mathcal{E}_ϕ , including the position processing module, the atom embedder, the edge embedder, and the cross processing module. **b** The structure of the decoder \mathcal{D}_θ , including the position processing module, the atom embedder, the edge embedder, and the message extraction module.

In the embedding process, the encoder \mathcal{E}_ϕ embeds a binary watermark $\mathbf{m} = (\mathbf{m}_1, \dots, \mathbf{m}_L) \in \{0, 1\}^{1 \times L}$ into the structure of the molecules, in which L is the length of the watermark. The embedding process leverages both the atom position \mathbf{p} and the node features \mathbf{h} to embed the watermark while preserving molecular properties. The watermark embedding process is formulated as follows:

$$\mathbf{p}' = \mathcal{E}_\phi(\mathbf{p}, \mathbf{h}, \mathbf{m}), \quad (1)$$

where $\mathbf{p}' = (\mathbf{p}'_1, \dots, \mathbf{p}'_N) \in \mathbf{R}^{N \times 3}$ is the embedded atom positions. Specifically, the encoder is designed to modify the atom positions while keeping the node features unchanged. After embedding the watermark, the embedded molecules can be represented as the geometries $\mathcal{G}' = \langle \mathbf{p}', \mathbf{h} \rangle \in \mathbf{R}^{N \times (3+d)}$.

3.1.1 Structure of Encoder

Fig. 5 (a) presents the structure of the encoder \mathcal{E}_ϕ , which is designed to embed watermarks without compromising the properties of embedded molecules. The encoder \mathcal{E}_ϕ is composed of the position processing module, the atom embedder, the edge embedder, and the cross processing module. We describe the basic functionality of the four modules as follows.

Position Processing Module: Given that each molecule contains only a few atoms, the redundant space for embedding a watermark is limited. To address this, the position processing module projects the atom positions \mathbf{p} into a high-dimensional space to generate the position features \mathbf{f}_p as follows:

$$\mathbf{f}_p = f_{\text{position}}(\mathbf{p}). \quad (2)$$

Since the atom position is represented as $\mathbf{p} = (\mathbf{p}_1, \dots, \mathbf{p}_N) \in \mathbf{R}^{N \times 3}$, the atom position batch \mathbf{p}^B with size of $(B, 1, N, 3)$ is first constructed, in which the batch size is set as $B = 64$. A series of convolutional operations is applied to map the batch \mathbf{p}^B to position features \mathbf{f}_p with size $(B, C, N, 3)$, in which channel dimension is set to $C = 64$. This transformation expands the representational capacity of the spatial data, providing additional redundancy for effective and robust watermark embedding.

Atom Embedder: The atom embedder leverages the node features \mathbf{h} to support the watermark embedding process. Specifically, it utilizes the atom type \mathbf{t} and atom charge \mathbf{c} to generate the atom features \mathbf{f}_a as follows:

$$\mathbf{f}_a = f_{\text{atom}}(\mathbf{t}, \mathbf{c}). \quad (3)$$

For a batch of molecules, the atom type batch \mathbf{t}^B is constructed with size of $(B, 1, N, e)$ and the atom charge batch \mathbf{c}^B is constructed with size of $(B, 1, N, 1)$. The atom type \mathbf{t} is represented as the one-hot vector, in which the length is defined by the number of atomic species $e \in \{5, 16\}$. The position embedding method in Transformer⁴⁷ is utilized to generate the sine and cosine positional embedding PE , where the atom number N determines the length of PE . The calculation of PE is defined as

follows:

$$PE_{(pos,i)} = \begin{cases} \sin(\frac{pos}{num^{i/d_{model}}}) & \text{if } \text{mod}(i,2) == 0, \\ \cos(\frac{pos}{num^{(i-1)/d_{model}}}) & \text{if } \text{mod}(i,2) == 1, \end{cases} \quad (4)$$

where $0 \leq i < d_{model}/2$, pos is the index of the position, and num is the maximum length of the position embedding. We set the dimension of PE as $d_{model} = 64$ in implementation. Following this, PE is repeated to the batch size as $(B, 1, N, d_{model})$. Considering the position embedding, the atom charge batch \mathbf{c}^B is mapped as follows:

$$\mathbf{c}^B = PE \circ \mathbf{c}^B, \quad (5)$$

where \circ calculate the Hadamard product and the resulting size is $(B, 1, N, d_{model})$. To align feature dimensions, a linear operation is applied to the atom type batch \mathbf{t}^B , mapping it into the latent space of the same dimension. Following this, the mapped atom charge batch \mathbf{c}^B and the atom type batch \mathbf{t}^B are concatenated in the last dimension. In this light, the combined representation is passed through a linear layer to produce atom features $\mathbf{f}_a \in \mathbb{R}^{B \times 1 \times N \times 3}$, matching the dimensionality of the position features \mathbf{f}_p .

Edge Embedder: To further enhance the watermark embedding process, the edge correlations between atoms are explicitly considered. The molecules are sensitive to spatial perturbations, and minor changes in atom positions can significantly alter interatomic distances, potentially exceeding chemical bond lengths and compromising molecular properties. To mitigate these issues, the distances between atoms are considered in the edge embedder to generate the edge features \mathbf{f}_e . In this way, the edge indexes \mathbf{e} , the atom features \mathbf{f}_a , and the atom positions \mathbf{p} are served as the inputs of the edge embedder:

$$\mathbf{f}_e = f_{edge}(\mathbf{e}, \mathbf{f}_a, \mathbf{p}). \quad (6)$$

For a batch of molecules, the edge index batch can be represented as \mathbf{e}^B with the size of $(B, 1, N, N-1)$. Given the high sensitivity of molecular structures to perturbations, we calculate the distance relationship between atoms to enhance the edge representations as follows:

$$\mathbf{a}_d = f_{agg}(\mathbf{e}, \mathbf{p}). \quad (7)$$

where f_{agg} represents the aggregation methods. Specifically, we use the summation (“SUM”) and averaging (“MEAN”) as the aggregation methods. The \mathbf{a}_d is the aggregated distance between atoms with the size of $(B, 1, N, 1)$. Following this, the atom features \mathbf{f}_a and aggregated distance \mathbf{a}_d are concatenated in the last dimension. This concatenated representation is then processed by a linear operation to produce the aggregated features \mathbf{f}'_a . Subsequently, the same position embedding method⁴⁷ is applied to generate the position embedding PE with the number of atoms N . Then, the aggregated features \mathbf{f}'_a and the position embedding PE are concatenated in the last dimension, which are passed through a series of linear layers with layer normalization. Finally, the final edge features $\mathbf{f}_e \in \mathbb{R}^{B \times 1 \times N \times 3}$ can be generated.

Cross Processing Module: Building upon the position features \mathbf{f}_p , the atom features \mathbf{f}_a and the edge features \mathbf{f}_e , the cross processing module integrates these representations with the watermark \mathbf{m} , generating the embedded atom positions $\mathbf{p}' = (\mathbf{p}'_1, \dots, \mathbf{p}'_N) \in \mathbb{R}^{N \times 3}$. The embedding process is defined as:

$$\mathbf{p}' = f_{cross}(\mathbf{f}_p, \mathbf{f}_a, \mathbf{f}_e, \mathbf{m}). \quad (8)$$

The watermark \mathbf{m} is a binary sequence with length L , which is expanded to match the dimensionality of the generated features. To this end, each bit in the watermark is replicated to construct the expanded watermark $\mathbf{m}^e \in \mathbb{R}^{B \times L \times N \times 3}$. The latent feature representation \mathbf{f}_c is then formed by concatenating the position features \mathbf{f}_p , the atom features \mathbf{f}_a , the edge features \mathbf{f}_e , and the expanded watermark \mathbf{m}^e along the channel dimension. This composite tensor is processed through three cross operations⁴⁸, followed by a self-attention mechanism⁴⁷ to generate the feature mask \mathbf{f}_m . The latent features \mathbf{f}_c are element-wise multiplied with \mathbf{f}_m , after which a convolutional layer is utilized to produce a position mask $\mathbf{p}_m \in \mathbb{R}^{B \times 1 \times N \times 3}$. Finally, the position mask \mathbf{p}_m and the original atom positions \mathbf{p} are added to generate the final embedded atom positions \mathbf{p}' . These strategies enhance feature interaction and ensure that the watermark is deeply embedded in a minimally invasive way.

3.1.2 Optimization of the Encoder

The four main components of the encoder \mathcal{E}_ϕ collaboratively embed the watermark \mathbf{m} into the atom position \mathbf{p} with the assistance of atom features \mathbf{h} , thereby generating the embedded geometries \mathcal{G}' . To ensure that the embedding process has a slight impact on the molecular structures and preserves molecular properties, the training objective aims to minimize the deviation between the original and embedded molecules. The encoder loss \mathcal{L}_E is defined to quantify the difference between the original and embedded molecules:

$$\mathcal{L}_E(\mathbf{p}, \mathbf{p}') = \max(|\mathbf{p} - \mathbf{p}'|^2) + \frac{1}{N} \sum_{i=1}^N \|\mathbf{p}_i - \mathbf{p}'_i\|_2^2, \quad (9)$$

where $\max(\cdot)$ and $\|\cdot\|_2$ calculate the maximum and the Euclidean norm of the input matrix, respectively. The encoder loss \mathcal{L}_E is composed of two complementary components that measure the deviation between the embedded atom position \mathbf{p}' and the original atom position \mathbf{p} :

1. **Maximum Distance:** Captures the largest positional shift among all atoms, serving as a strict upper bound on distortion. However, this term is non-differentiable, making it unsuitable for gradient-based optimization.
2. **Euclidean Norm:** Measures the overall displacement using the Euclidean norm ℓ_2 , which is differentiable and thus enables effective gradient descent during training.

By combining these two complementary components, the loss function ensures that the encoder parameters ϕ are optimized to minimize structural perturbations. This approach limits the maximum distortion with smooth optimization, establishing an effective method to maintain the molecular properties after embedding watermarks.

3.2 Watermark Extraction

The watermark extraction utilizes the decoder \mathcal{D}_θ to extract the embedded watermark from the molecules $\mathcal{G}' = \langle \mathbf{p}', \mathbf{h} \rangle \in \mathbf{R}^{N \times (3+d)}$. Specifically, the molecular properties remain unchanged after processing by SE(3) transformations, indicating that the processed molecules are also protected by the copyright. Therefore, the decoder \mathcal{D}_θ must be robust against SE(3) transformations, which is reflected in the high bit accuracy of extracting watermarks from processed molecules. This robustness is essential for copyright protection in real-world scenarios, where molecules may be processed, visualized, or manipulated into various spatial conformations.

To achieve robustness, we first identify and extract the SE(3) invariant features from the molecules. Within the molecule geometries \mathcal{G} , the node features \mathbf{h} are invariant to SE(3) transformations, while the atom positions \mathbf{p} are variant. Therefore, we focus on extracting SE(3) invariant features from the atom positions \mathbf{p} , enabling the decoder \mathcal{D}_θ to accurately extract the embedded watermark from the transformed molecules. The SE(3) invariant features must satisfy the following criteria:

$$\mathcal{F}(\mathbf{p}) = \mathcal{F}(\mathbf{p}\mathbf{A} + \mathbf{T}), \quad (10)$$

where $\mathcal{F}(\cdot)$ denotes the feature extraction function, \mathbf{A} is a linear transformation matrix (*e.g.*, rotation or reflection), and \mathbf{T} is a translation vector. Through empirical analysis, we identify that the Euclidean distances between atom positions satisfy the relationship in Eq. 10. The distance matrix captures the internal geometry of the molecules while discarding the absolute orientation and position in space. As such, we utilize the Euclidean distance matrix $\mathbf{d} \in \mathbf{R}^{N \times N}$ as the SE(3) invariant features. For the i -th and j -th atoms, the distance $d_{i,j}$ is calculated as follows:

$$d_{i,j} = \sqrt{(x_i - x_j)^2 + (y_i - y_j)^2 + (z_i - z_j)^2} \quad (11)$$

where (x_i, y_i, z_i) and (x_j, y_j, z_j) are the coordinates of the i -th and the j -th atoms, respectively.

The distance matrix \mathbf{d} is a symmetric matrix that is rich in structural information. Directly extracting the embedded watermark from \mathbf{d} may lead to numerical instability, which may degrade the performance of the decoder \mathcal{D}_θ . To alleviate this issue, we utilize the MDS method⁴⁹ to convert the distance matrix \mathbf{d} into $\hat{\mathbf{p}} \in \mathbf{R}^{N \times 3}$, which approximates the embedded atom positions \mathbf{p}' . This transformation allows the decoder to operate on coordinate-level features while preserving SE(3) invariance, thereby improving the bit accuracy.

3.2.1 Multi Dimensional Scaling

The details of the MDS method are described as follows. At first, the distance matrix \mathbf{d} is utilized to construct the centered distance matrix $\mathbf{B} \in \mathbf{R}^{N \times N}$ as follows:

$$\mathbf{B} = -\frac{1}{2}\mathbf{J}\mathbf{d}^2\mathbf{J} \quad (12)$$

where \mathbf{d}^2 denotes the square of the elements within the distance matrix \mathbf{d} . The centered matrix $\mathbf{J} \in \mathbf{R}^{N \times N}$ is defined as follows:

$$\mathbf{J} = \mathbf{I} - \frac{1}{n}\mathbf{1}\mathbf{1}^T. \quad (13)$$

Here, $\mathbf{I} \in \mathbf{R}^{N \times N}$ represents the identity matrix and $\mathbf{1} \in \mathbf{R}^{N \times 1}$ denotes the matrix of ones. The eigenvalue decomposition is then performed on the centered distance matrix \mathbf{B} to calculate the eigenvalues and the eigenvectors:

$$\mathbf{B} = \mathbf{V}\mathbf{\Lambda}\mathbf{V}^T, \quad (14)$$

where $\Lambda \in \mathbf{R}^{N \times N}$ is the eigenvalue matrix and $\mathbf{V} \in \mathbf{R}^{N \times N}$ is the eigenvector matrix.

After decomposing the eigenvalues, the top k largest eigenvalues and the corresponding eigenvectors are utilized to calculate the recovered atom position $\hat{\mathbf{p}}$ as follows:

$$\hat{\mathbf{p}} = \mathbf{V}_k \Lambda_k^{1/2}, \quad (15)$$

where $\Lambda_k \in \mathbf{R}^{k \times k}$ is the diagonal matrix composed of the top k eigenvalues, and $\mathbf{V}_k \in \mathbf{R}^{k \times k}$ is the matrix containing the corresponding top k eigenvectors. The dimension k is set to 3 to ensure that $\hat{\mathbf{p}}$ are consistent with \mathbf{p}' in dimension.

3.2.2 Structure of Decoder

After converting the distance matrix \mathbf{d} into the recovered atom position $\hat{\mathbf{p}}$ by using the MDS method, the decoder \mathcal{D}_θ is employed to extract the embedded watermark $\mathbf{m}' = (\mathbf{m}'_1, \dots, \mathbf{m}'_L) \in \mathbf{R}^{1 \times L}$. The extraction process is expressed as follows:

$$\mathbf{m}' = \mathcal{D}_\theta(\hat{\mathbf{p}}, \mathbf{h}), \quad (16)$$

where the node features \mathbf{h} are utilized to assist the watermark extraction.

Fig. 5 (b) illustrates the architecture of the decoder \mathcal{D}_θ , which comprises four main components: the position mapping module, the atom embedder, the edge embedder, and the extraction module. While the atom embedder and edge embedder share the same structures as the counterparts in the encoder, they are trained with different parameters. Accordingly, we only describe the extraction module, which is responsible for extracting the embedded watermark from the processed molecules.

Extraction Module: This module is designed to extract the embedded watermark with high bit accuracy. The previous modules have generated the embedded position features \mathbf{f}'_p , the atom features \mathbf{f}_a , and the edge features \mathbf{f}_e . The watermark \mathbf{m}' is extracted as follows:

$$\mathbf{m}' = f_{\text{extract}}(\mathbf{f}'_p, \mathbf{f}_a, \mathbf{f}_e). \quad (17)$$

Initially, the generated features (\mathbf{f}'_p , \mathbf{f}_a , and \mathbf{f}_e) are concatenated along the channel dimension to form the latent representation \mathbf{f}_c , which is then processed through three cross operations to effectively integrate spatial and semantic information for watermark extraction. To align with the target watermark length L , an adaptive average pooling strategy is utilized to reshape the output features into $(B, L, 1, 1)$. Finally, the extracted watermark \mathbf{m}' is obtained by applying an element-wise rounding operation to binarize the pooled features.

3.2.3 Optimization of the Decoder

Leveraging the MDS method and the decoder \mathcal{D}_θ , the watermark \mathbf{m}' can be extracted. To enhance the performance of the decoder \mathcal{D}_θ , the difference between the extracted watermark \mathbf{m}' and the original watermark \mathbf{m} is minimized to improve the extraction accuracy. The difference is quantified by using the Euclidean norm ℓ_2 between \mathbf{m}' and \mathbf{m} , and the decoder loss \mathcal{L}_D is expressed as follows:

$$\mathcal{L}_D(\mathbf{m}, \mathbf{m}') = \frac{1}{L} \sum_{i=1}^L \|\mathbf{m}_i - \mathbf{m}'_i\|_2^2. \quad (18)$$

During training, the decoder loss \mathcal{L}_D is minimized to optimize the decoder parameters θ , thereby improving the accuracy of watermark extraction through a learnable strategy.

3.3 Training Objective

The proposed watermarking method is a learnable, end-to-end model for copyright protection of molecules, in which the training objective is to minimize both the encoder loss and the decoder loss. We perform Adam optimization⁵⁰ with default hyperparameters on the model parameters ϕ and θ . The overall training objective is defined over the distribution of the molecules and the watermarks:

$$\min_{\phi, \theta} \mathbb{E}_{(\mathbf{p}, \mathbf{m})} [\lambda_E \mathcal{L}_E(\mathbf{p}, \mathbf{p}') + \lambda_D \mathcal{L}_D(\mathbf{m}, \mathbf{m}')], \quad (19)$$

where λ_E and λ_D are the relative weights of the encoder loss and the decoder loss, respectively.

The training process is designed to jointly optimize the encoder \mathcal{E}_ϕ and decoder \mathcal{D}_θ , with the objective of maintaining the properties of the embedded molecules while improving the bit accuracy of the extracted watermark. To achieve this, we introduce a carefully balanced training strategy, in which the relative weights λ_E and λ_D are dynamically changed to control the

importance of optimizing the encoder versus the decoder during training. Specifically, the definitions of λ_E and λ_D are given as follows:

$$\lambda_E = \rho + \beta \times \left\lfloor \frac{t}{f} \right\rfloor, \quad (20)$$

and

$$\lambda_D = \delta \times (1 - \gamma). \quad (21)$$

We set the hyperparameters as $\rho = 0.01$, $\beta = 0.25$, and $\delta = 100$. In Eq. 20, t denotes the current training epoch, and f defines the interval to increase λ_E , which is typically set to $f = 50$. As the training epoch increases, the weight λ_E increases linearly, emphasizing the optimization of the encoder gradually. Meanwhile, the bit accuracy $\gamma \in [0, 1]$ also increases, adjusting the weight λ_D through the bit accuracy feedback. Notably, λ_D is initialized with a higher value than λ_E , prioritizing the optimization of the decoder \mathcal{D}_θ in the early training epochs to ensure high watermark extraction accuracy. When γ increases, λ_D decreases rapidly to a level comparable to λ_E , so that the encoder \mathcal{E}_ϕ can be optimized to maintain the molecular properties. In this way, the adaptive weighting strategy enables the model to maintain the structural fidelity of molecules and improve the extraction accuracy of the watermark throughout training.

In conclusion, the proposed optimization strategy achieves a dynamic balance between bit accuracy and molecular properties by adaptively adjusting the relative weights. The decoder weight is modulated based on the real-time change in bit accuracy. When the bit accuracy decreases, the decoder weight increases, optimizing the decoder to improve the watermark extraction accuracy. Conversely, the encoder weight increases progressively with training epochs, reducing the perturbation introduced by watermark embedding. The total loss is computed as a weighted average of the encoder and decoder losses, enabling the optimization of the proposed watermarking method. During the early training epoch, the model emphasizes the accuracy of watermark extraction, while in later stages, it gradually reduces the impact of embedding watermarks on molecular structures. In this way, the dynamic training strategy ultimately facilitates robust watermark embedding while maintaining molecular properties.

Data availability

The QM9 dataset is available at <http://quantum-machine.org/datasets/>. The GEOM-DEUG dataset is available at <https://dataverse.harvard.edu/dataset.xhtml?persistentId=doi:10.7910/DVN/JNGTDF>. The RCSB Protein Data Bank dataset is available at <https://www.rcsb.org/>.

Code availability

The source codes are available via GitHub at <https://github.com/RunwenHu/WMM>.

Contributions

R.H., P.C., K.D., and S.W. conceived the study and designed the experiments. R.H. and P.C. conducted computational experiments and theoretical analyses. P.C. and K.D. assisted with some experiments and analyses. R.H., P.C., K.D., and S.W. wrote the paper.

Competing interests

The authors declare no competing interests.

References

1. Yang, K. K., Wu, Z. & Arnold, F. H. Machine-learning-guided directed evolution for protein engineering. *Nat. Methods* **16**, 687–694 (2019).
2. Luo, Y. *et al.* Ecnnet is an evolutionary context-integrated deep learning framework for protein engineering. *Nat. Commun.* **12**, 5743 (2021).
3. Pandey, M. *et al.* The transformational role of gpu computing and deep learning in drug discovery. *Nat. Mach. Intell.* **4**, 211–221 (2022).
4. Yu, M. *et al.* Deep learning large-scale drug discovery and repurposing. *Nat. Comput. Sci.* **4**, 600–614 (2024).

5. De Almeida, A. F., Moreira, R. & Rodrigues, T. Synthetic organic chemistry driven by artificial intelligence. *Nat. Rev. Chem.* **3**, 589–604 (2019).
6. Gebauer, N., Gastegger, M. & Schütt, K. Symmetry-adapted generation of 3d point sets for the targeted discovery of molecules. *Adv. neural information processing systems* **32** (2019).
7. Luo, Y. & Ji, S. An autoregressive flow model for 3d molecular geometry generation from scratch. In *International conference on learning representations (ICLR)* (2022).
8. Xu, M., Powers, A. S., Dror, R. O., Ermon, S. & Leskovec, J. Geometric latent diffusion models for 3d molecule generation. In *International Conference on Machine Learning*, 38592–38610 (PMLR, 2023).
9. Anand, N. & Achim, T. Protein structure and sequence generation with equivariant denoising diffusion probabilistic models. *arXiv preprint arXiv:2205.15019* (2022).
10. Peng, X., Guan, J., Liu, Q. & Ma, J. Moldiff: Addressing the atom-bond inconsistency problem in 3d molecule diffusion generation. *arXiv preprint arXiv:2305.07508* (2023).
11. Graves, A., Srivastava, R. K., Atkinson, T. & Gomez, F. Bayesian flow networks. *arXiv preprint arXiv:2308.07037* (2023).
12. Song, Y. *et al.* Unified generative modeling of 3d molecules with bayesian flow networks. In *The Twelfth International Conference on Learning Representations* (2023).
13. Qu, Y. *et al.* Molcraft: Structure-based drug design in continuous parameter space. *arXiv preprint arXiv:2404.12141* (2024).
14. Atkinson, T. *et al.* Protein sequence modelling with bayesian flow networks. *Nat. Commun.* **16**, 3197 (2025).
15. Guloglu, B. *et al.* Abbf2: A flexible antibody foundation model based on bayesian flow networks. *bioRxiv* 2025–04 (2025).
16. Segler, M. H., Preuss, M. & Waller, M. P. Planning chemical syntheses with deep neural networks and symbolic ai. *Nature* **555**, 604–610 (2018).
17. Shafiq, M., Thakre, K., Pandurangan, R. & Lalitha, R. V. S. Generative ai designs the next generation of smart materials from pixels to products. *The Int. J. Adv. Manuf. Technol.* 1–12 (2025).
18. Goswami, L., Deka, M. K. & Roy, M. Artificial intelligence in material engineering: A review on applications of artificial intelligence in material engineering. *Adv. Eng. Mater.* **25**, 2300104 (2023).
19. Cotton, D. R., Cotton, P. A. & Shipway, J. R. Chatting and cheating: Ensuring academic integrity in the era of chatgpt. *Innov. education teaching international* **61**, 228–239 (2024).
20. Ho, J., Jain, A. & Abbeel, P. Denoising diffusion probabilistic models. *Adv. neural information processing systems* **33**, 6840–6851 (2020).
21. Meng, C. *et al.* Sdedit: Guided image synthesis and editing with stochastic differential equations. *arXiv preprint arXiv:2108.01073* (2021).
22. Li, X., Thickstun, J., Gulrajani, I., Liang, P. S. & Hashimoto, T. B. Diffusion-lm improves controllable text generation. *Adv. Neural Inf. Process. Syst.* **35**, 4328–4343 (2022).
23. Corvi, R., Cozzolino, D., Poggi, G., Nagano, K. & Verdoliva, L. Intriguing properties of synthetic images: from generative adversarial networks to diffusion models. In *Proceedings of the IEEE/CVF conference on computer vision and pattern recognition*, 973–982 (2023).
24. Xu, Q. *et al.* Exposing fake images generated by text-to-image diffusion models. *Pattern Recognit. Lett.* **176**, 76–82 (2023).
25. Liu, Y. *et al.* Sora: A review on background, technology, limitations, and opportunities of large vision models. *arXiv preprint arXiv:2402.17177* (2024).
26. Wang, M. *et al.* A call for built-in biosecurity safeguards for generative ai tools. *Nat. Biotechnol.* **43**, 845–847 (2025).
27. Zhu, J., Kaplan, R., Johnson, J. & Fei-Fei, L. Hidden: Hiding data with deep networks. In *Proceedings of the European Conference on Computer Vision (ECCV)*, 657–672 (2018).
28. Liu, Y., Guo, M., Zhang, J., Zhu, Y. & Xie, X. A novel two-stage separable deep learning framework for practical blind watermarking. In *Proceedings of the 27th ACM International Conference on Multimedia*, 1509–1517 (2019).
29. Jia, Z., Fang, H. & Zhang, W. Mbrs: Enhancing robustness of dnn-based watermarking by mini-batch of real and simulated jpeg compression. In *Proceedings of the 29th ACM International Conference on Multimedia*, 41–49 (2021).

30. Fang, H. *et al.* De-end: decoder-driven watermarking network. *IEEE Transactions on Multimed.* (2022).
31. Huang, J. *et al.* Arwgan: Attention-guided robust image watermarking model based on gan. *IEEE Transactions on Instrumentation Meas.* (2023).
32. Zhang, Z. *et al.* Foldmark: Protecting protein generative models with watermarking. *bioRxiv* 2024–10 (2024).
33. Chen, Y. *et al.* Enhancing privacy in biosecurity with watermarked protein design. *Bioinformatics* btaf141 (2025).
34. Ramakrishnan, R., Dral, P. O., Rupp, M. & Von Lilienfeld, O. A. Quantum chemistry structures and properties of 134 kilo molecules. *Sci. data* **1**, 1–7 (2014).
35. Axelrod, S. & Gomez-Bombarelli, R. Geom, energy-annotated molecular conformations for property prediction and molecular generation. *Sci. Data* **9**, 185 (2022).
36. Anderson, B., Hy, T. S. & Kondor, R. Cormorant: Covariant molecular neural networks. *Adv. neural information processing systems* **32** (2019).
37. Hooeboom, E., Satorras, V. G., Vignac, C. & Welling, M. Equivariant diffusion for molecule generation in 3d. In *International conference on machine learning*, 8867–8887 (PMLR, 2022).
38. Wu, L., Gong, C., Liu, X., Ye, M. & Liu, Q. Diffusion-based molecule generation with informative prior bridges. *Adv. neural information processing systems* **35**, 36533–36545 (2022).
39. Landrum, G. *et al.* Rdkit: Open-source cheminformatics (2006).
40. O’Boyle, N. M. *et al.* Open babel: An open chemical toolbox. *J. cheminformatics* **3**, 1–14 (2011).
41. Michaud-Agrawal, N., Denning, E. J., Woolf, T. B. & Beckstein, O. Mdanalysis: a toolkit for the analysis of molecular dynamics simulations. *J. computational chemistry* **32**, 2319–2327 (2011).
42. Gowers, R. J. *et al.* Mdanalysis: a python package for the rapid analysis of molecular dynamics simulations. Tech. Rep., Los Alamos National Laboratory (LANL), Los Alamos, NM (United States) (2019).
43. Ertl, P., Rohde, B. & Selzer, P. Fast calculation of molecular polar surface area as a sum of fragment-based contributions and its application to the prediction of drug transport properties. *J. medicinal chemistry* **43**, 3714–3717 (2000).
44. Berman, H., Henrick, K. & Nakamura, H. Announcing the worldwide protein data bank. *Nat. structural & molecular biology* **10**, 980–980 (2003).
45. Trott, O. & Olson, A. J. Autodock vina: improving the speed and accuracy of docking with a new scoring function, efficient optimization, and multithreading. *J. computational chemistry* **31**, 455–461 (2010).
46. Eberhardt, J., Santos-Martins, D., Tillack, A. F. & Forli, S. Autodock vina 1.2. 0: New docking methods, expanded force field, and python bindings. *J. chemical information modeling* **61**, 3891–3898 (2021).
47. Vaswani, A. Attention is all you need. *Adv. Neural Inf. Process. Syst.* (2017).
48. Huang, G., Liu, Z., Van Der Maaten, L. & Weinberger, K. Q. Densely connected convolutional networks. In *Proceedings of the IEEE conference on computer vision and pattern recognition*, 4700–4708 (2017).
49. Carroll, J. D. & Arabie, P. Multidimensional scaling. *Meas. judgment decision making* 179–250 (1998).
50. Kingma, D. P. & Ba, J. L. Adam: a method for stochastic optimization. In *International Conference on Learning Representations* (2014).